This article has been accepted for publication in a future issue of this journal, but has not been fully edited. Content may change prior to final publication. Citation information: DOI 10.1109/ACCESS.2020.3041633, IEEE Access

IEEE Access
Multidisciplinary | Rapid Review | Open Access Journal

Date of publication xxxx 00, 0000, date of current version xxxx 00, 0000.

Digital Object Identifier 10.1109/ACCESS.2020.DOI

Lens Antenna Subarrays in mmWave Hybrid MIMO Systems

MURAT KARABACAK[1], (Member, IEEE), HÜSEYIN ARSLAN[1], (Fellow, IEEE), AND GOKHAN MUMCU[1], (Senior Member, IEEE).

[1]Department of Electrical Engineering, University of South Florida, Tampa, FL (e-mail: murat@usf.edu, arslan@usf.edu, mumcu@usf.edu)

Corresponding author: Murat Karabacak (e-mail: murat@usf.edu).

This work was supported by the U.S. National Science Foundation Award ECCS-1923857.

ABSTRACT Data rate and energy efficiency performance of mmWave wireless communication systems consisting of a new lens antenna subarray (LAS) based hybrid multiple input multiple output (MIMO) architecture is investigated. The LAS architecture degenerates into traditional hybrid MIMO architecture (TA) or single lens antenna array architecture (SLA) when the lens diameter of the subarray is reduced or enlarged, respectively. It is shown that under mmWave channel scattering conditions, LAS architecture operates with a data rate approaching that of TA while significantly exceeding the data rate of the SLA. Due to the reduced hardware complexity and power consumption, LAS architectures operate with a significantly improved energy efficiency. In an example system consisting of 64 and 16 transmitter and receiver antennas with 2 RF chains, it is shown that the LAS architecture operates with $2\times$ energy efficiency and 98% spectrum efficiency. In a larger hybrid MIMO antenna systems, LAS architecture is expected to benefit even more.

INDEX TERMS MIMO, beamforming, lens antenna, large antenna array, subarray, mmWave.

I. INTRODUCTION

Multimedia driven technologies and multifunctional wireless devices have pushed the existing wireless systems to their limits in traditionally utilized spectrum and increased the desire to operate at higher frequency bands [1], [2]. Federal Communications Commission (FCC) has already stepped forward and opened millimeter-wave (mmWave) band for future radio access [3]. It is well known that in mmWave bands, the communication signals suffer from high propagation loss [4], [5]. On the other hand, as an important feature of mmWave bands, the smaller wavelengths make it possible to practically pack a large number of antennas with reasonable form factors. Thus, mmWave communication can provide directional transmission with high gain antenna arrays. Beamforming algorithms are used to optimize transmission direction and overcome harsh channel conditions (i.e., high attenuation, blockage) [6]–[9]. Unlike the lower frequency bands, cost and power consumption of hardware components in mmWave band limits the widespread utilization of mmWave communication systems. This problem is further exacerbated with the desire of including radio frequency (RF) chains and analog to digital (ADC) / digital to analog (DAC) converters per antenna element since high gain antenna arrays consist of many elements. Thus, hybrid multiple input multiple output (MIMO) architecture that packs fewer RF chains at the back of the high gain antenna array has attracted great interest over the recent years [10].

Hybrid MIMO architecture prevents usage of many RF chains and ADC/DACs [10]–[14]. Although number of RF chains are less than the number of antenna elements, the complexity and power consumption of hybrid MIMO architecture continues to be challenging for hardware implementations due to need for large number of analog RF components (e.g. phase shifters). The implementation and power consumption challenges increase for larger antenna arrays such as 256 antenna elements [15] or more to satisfy necessary system performance. In addition to hardware complexity and cost, recent studies demonstrate that the DC power consumed by the phase shifters (and their variable gain amplifiers) becomes critical [16], [17]. This problem is exacerbated in the traditional hybrid MIMO architecture (TA) since the number of phase shifters becomes multiple of the number of RF chains and antennas employed within the architecture. Therefore, several alternative architectures that reduce the total number of phase shifters have been recently investigated with regards to their spectrum and energy efficiencies [17]. These alternative architectures have reduced the total number of phase shifters with combinations of replacing them with less power demanding RF switches, implementing different signal summation paths, and grouping elements into smaller

This work is licensed under a Creative Commons Attribution 4.0 License. For more information, see https://creativecommons.org/licenses/by/4.0/

This article has been accepted for publication in a future issue of this journal, but has not been fully edited. Content may change prior to final publication. Citation information: DOI 10.1109/ACCESS.2020.3041633, IEEE Access

phased arrays. However, these investigations have shown that although alternative architectures consume less power (due to the removal of phase shifters), they operate with less spectrum efficiency. Hence, the energy efficiency (i.e. data rate / power consumption) have remained very similar to the TA [17]. A different approach to the problem is presented in [18], [19] using a few bit ADC receivers, where in the receiver a cost efficient ADC with less number of quantization levels is implemented.

The main issue with the proposed alternative hybrid MIMO architectures in [17] is related to their inability to generate the same antenna gain and similar beamforming as TA could do. For example, one classical approach for reducing the total number of phase shifters in a phased antenna array is the subarraying technique [20]. Another example is to implement adaptive subarray systems to optimize the precoding architecture depending on the channel conditions [21]–[23]. However, classical subarraying significantly reduces the beam steering range that can be achieved without grating lobes. Consequently, although the subarray may operate as well as a TA in line-of-sight (LOS) communications falling within a narrow scan range, it cannot provide a large scan range and demonstrate full capability to constructively add the multipath scattering with optimum coefficients. On the other hand, single lens antenna array architecture (SLA) provides a similar capability to TA. They consist of an electrically large lens with antenna elements placed at the focal plane. Switching the excitation element also switches the radiated beam. The beam is high in gain and can be steered over a large angle. Since beam steering is performed with switches, hardware implementation is simplified and power consumption is reduced, typically at the expense of a larger antenna structure. Consequently, a number of studies have proposed usage of SLAs in mmWave wireless communication systems [24]–[28]. Reference [24] investigates SLA with 1 RF chain for mmWave systems. In [25], SLA supporting RF chains that are much fewer in number than the total number of antennas is investigated for MIMO communications. Reference [29] provides multi-user extension to the SLA. In [27], pre-compensation of path delays is proposed to implement low complexity single carrier transmission. In [28], wide band beam selection algorithm is presented to improve sum-rate of the system.

The main drawbacks of SLAs can be considered to be their larger size and limitation for the beamforming precoding. In SLA, an RF chain gets connected to only one antenna element at a given time. In multipath environment, this prevents to implement a precoder/combiner that will optimize the shape of the beam and related coefficients to constructively combine signals arriving from multipaths. Hence, SLA is expected to underperform in spectrum efficiency in a multipath environment. In this paper, we propose to investigate spectrum and energy efficiency of a recently introduced architecture: lens antenna subarrays (LAS) [30], [31]. LAS architecture is shown in Fig. 1 and compared to the TA with Fig. 2. Signal from an RF chain (out of a total of N^{RF} chains) gets connected to L discrete lenses after passing from a phase shifter. Within the lens, the signal gets delivered to an antenna element by a RF switch network. The total number of antennas is N where $M = N/L$ denotes the number of antennas per lens. The total physical footprint of the lenses are approximately equal to the physical size of the half-wave spaced N antenna elements so that the TA and LAS architectures exhibit similar antenna gains. The total number of phase shifters are reduced by a factor of M. However, despite this reduction, each LAS maintains electronic beam-steering capability. Hence, the LAS architecture can potentially provide similar beam steering range with the TA and SLA. In fact, one can consider LAS architecture to be degenerating into a TA and SLA with the choices of $M = 1$ and $M = N$, respectively. Power consumption is expected to be reduced as M increases towards the SLA, however, this will negatively impact the spectrum efficiency in multipath environments. In contrast, reducing M will increase power consumption, but also increase its spectrum efficiency.

In this paper, we demonstrate for the first time that the proper choice of M can be utilized to obtain a better energy efficiency (i.e. data rate per power consumption) in mmWave communication systems as opposed to the conventional wisdom of using TA or SLA. Contributions of this paper can be summarized as

- For the first time, spectrum and energy efficiency of LAS architecture is investigated.
- Multiple stream and multiple RF chain scenarios for the LAS architecture are presented.
- The LAS architecture is evaluated with exhaustive search search algorithms to prove its capabilities.
- The performance of the LAS architecture is investigated within varying scattering environments to demonstrate its capabilities over SLA.

Section II describes the LAS architecture, wireless channel model, and system model. Section III demonstrates the performance of LAS architecture. Specifically by considering a mmWave propagation channel which consist of 6 clusters with 8 rays per cluster, it is shown that a mmWave system employing LAS architecture in its transmitter and receiver can operate with $2\times$ energy efficiency and 98% spectrum efficiency as compared to usage of TA.

Notation: Matrices are denoted by bold uppercase letters (e.g. $\boldsymbol{A}$), and vectors are denoted by bold lowercase letters (e.g. $\boldsymbol{a}$). $\boldsymbol{A}^H$ and $\boldsymbol{a}^T$ denote the Hermitian (conjugate transpose) of matrix $\boldsymbol{A}$ and regular transpose operation of $\boldsymbol{a}$, respectively.

II. SYSTEM MODEL

A. LENS ANTENNA SUBARRAY (LAS)

Dividing a large phased antenna array into subarrays for reducing the total number of phase shifters and simplifying the back-end electronics is a well-recognized concept [20].

This work is licensed under a Creative Commons Attribution 4.0 License. For more information, see https://creativecommons.org/licenses/by/4.0/

This article has been accepted for publication in a future issue of this journal, but has not been fully edited. Content may change prior to final publication. Citation information: DOI 10.1109/ACCESS.2020.3041633, IEEE Access

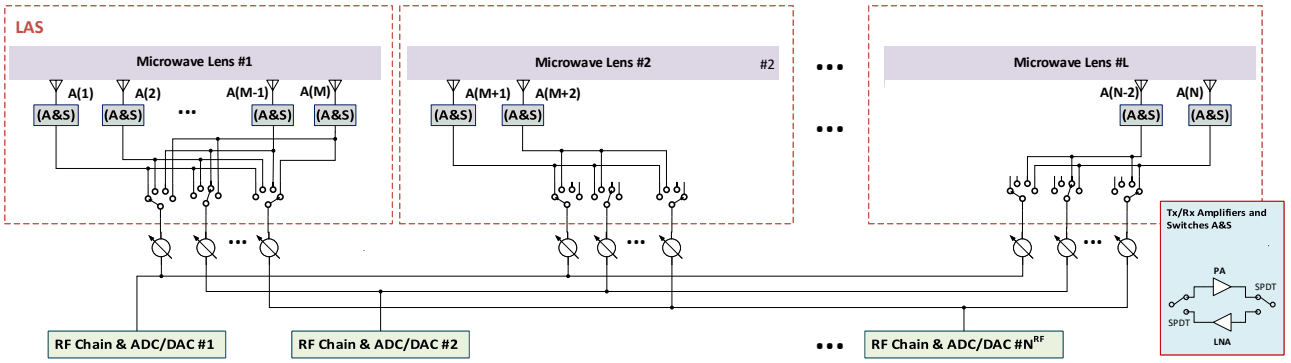


FIGURE 1. Lens antenna subarray (LAS) hybrid MIMO architecture.

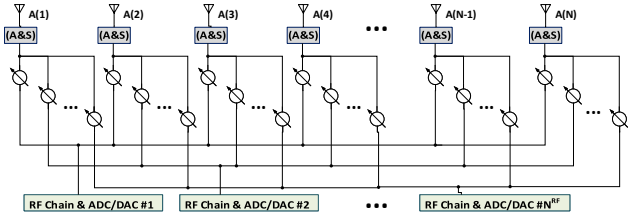


FIGURE 2. Traditional hybrid MIMO architecture (TA).

In this case, array factor (AF) of the antenna can be written as $AF = AF_pAF_s$, where AF_p and AF_s stand for the primary and secondary AFs corresponding to the subarray and array of subarrays, respectively. The absence of phase shifters causes AF_p to lose its electronic beam-steering capability, while AF_s exhibits grating lobes due to the large spacing among the subarrays. Consequently, for large scan angles, grating lobes of AF_s enter into the visible range and cause a limited scan range with large side lobe levels (SLLs). Overlapping and interlacing subarrays improves scan range and SLL [20], [32]. However, these techniques still underperform in comparison to the traditional phased arrays. Additionally, these techniques present implementation challenges. For example, overlapping requires smaller inter-element spacing and multiple RF crossings in the feed network – not easily scalable to mmWaves. Amplitude control and randomization of subarray antenna grouping are promising to enhance performance [33], but scan range is still well below the traditional phased array. Importantly, amplitude control is performed with variable gain amplifiers – implying significant power consumption for massive MIMO arrays [34].

LAS architecture places microwave lenses over the subarrays. Antenna elements of the subarray are located in the focal plane of the lens. Consequently, each antenna within the subarray becomes associated with a beam pointed towards a different angular direction. The LAS architecture therefore necessitates to include a switch network per a subarray as well to perform antenna selection based on desired angular beam direction. These architectural modifications allows AF_p to gain its electronic beam-steering capability. Hence, AF_pAF_s can perform without issues of grating lobes when AF_p and AF_s are properly steered through the switch network and phase shifter included under each lens. Due to AF_p gaining electronic beam-steering capability, LAS based antenna offers a large scan range as compared to other subarray techniques. The LAS architecture is flexible for making trade-offs between the total number of switches and phase shifters by adjusting the number of antennas placed under each lens (L).

LAS architecture is presented in Fig. 1. In a particular LAS architecture example, the variables were selected as $N = 20$ antenna elements, $L = 5$ lenses, $M = N/L = 4$, $N^{RF} = 1$ and radiation performance was investigated [30]. This was a 1D linear array implementation of the LAS architecture. It was designed with the objectives of meeting the radiation efficiency and aperture efficiency (i.e. half-power beamwidth (HPBW)) performance of a traditional $N = 20$ element $\lambda/2$ spaced 1D linear phased antenna array (i.e. > 15 dBi gain, and 80% radiation efficiency based on full wave simulation of traditional array). These objectives were met with an SLL below 9 dB and scan range of $\pm 37.5°$. In [35], this concept was extended to 2D beam steering by using extended hemispherical dielectric lenses with variables selected as $N = 119$ antenna elements, $L = 7$ lenses, $M = N/L = 17$, and $N^{RF} = 1$. The antenna operated with 19.8 dBi gain, $10°$ degree HPBW, SLL below -9.7 dB, and a scan range approaching $\pm 45°$. As shown in the table provided in [35], LAS architecture significantly enhances the scan range over other subarrays.

1) Scan Range Assumption

Typically, TAs operate with scan ranges of $\pm 45°$ and can approach to $\pm 60°$ with careful design considerations (such as suppression of surface waves). As a new architecture, LAS architecture may have potential to match this scan range in future and has already demonstrated $\approx \pm 45°$ [30], [35]. As stated above, these recent publications realize LAS using extended hemispherical dielectric lenses with antennas

This work is licensed under a Creative Commons Attribution 4.0 License. For more information, see https://creativecommons.org/licenses/by/4.0/

This article has been accepted for publication in a future issue of this journal, but has not been fully edited. Content may change prior to final publication. Citation information: DOI 10.1109/ACCESS.2020.3041633, IEEE Access

located in focal plane. Different lens types and/or focal arc positioning of antenna elements can be investigated to further improve the scan range performances. Based on these observations, in the system analysis, scan range of TA and LAS architectures will be treated as equal to each other as $\pm 45°$.

2) Radiated Beam Assumption

Uniform TAs operate with -13 dB SLL. LAS architecture is already shown to provide ≈ -10 dB SLL in recent publications [30], [35]. In addition, antenna gain obtained from LAS architecture is shown to be comparable to that of the TA. Due to the low level of SLL and on-going research in the design of LAS architectures towards improving performance, system analysis will treat the SLL level of LAS to be equal of TA for simplicity. Under equal SLL, equal scan range, and equal HPBW assumption, the radiated beam from a LAS architecture consisting of M antennas will be equal to the beam radiated by an M element half-wavelength spaced TA. Therefore, in the system analysis, the LAS can be replaced with an M element TA with beam steering vector of

$$\mathbf{v}^m = [e^{-j\pi(M/2)\sin(\theta_m)}, e^{-j\pi(M/2-1)\sin(\theta_m)}, e^{-j\pi(M/2-2)\sin(\theta_m)}, \ldots, e^{-j\pi(-M/2)\sin(\theta_m)}]^T, \quad (1)$$

where $\theta_m = \pi/4 - (m-1)\pi/2/(M-1)$ is the direction of the radiating beam from LAS while $m = 1, 2, ...M$ indicates the antenna selected with the switch network. Radiated beam directions from the LAS architecture takes discrete values due to the discrete number of antenna elements. Location of these elements are designed to generate beams with equal θ spacing.

B. SYSTEM MODEL

We assume that the LAS architecture shown in Fig. 1 is used in a single-user mmWave system. The transmitter with N_t antennas, L_t lenses, N_t^{RF} chains transmits N_s data streams to the receiver with N_r antennas, L_r lenses, N_r^{RF} chains where $N_s \leq N_t^{RF} \leq N_t$ and $N_s \leq N_r^{RF} \leq N_r$. Based on hybrid beamforming equations given in [14], and considering narrowband frequency-flat channel model, the received signal can be given as

$$\mathbf{r} = \sqrt{\rho}\mathbf{H}\mathbf{F}\mathbf{s} + \mathbf{n} \quad (2)$$

where $\mathbf{r}$ is the $N_r \times 1$ received signal vector, $\mathbf{H}$ is the $N_r \times N_t$ channel matrix, $\mathbf{F}$ is the $N_t \times N_s$ precoder matrix, $\mathbf{s}$ is the $N_s \times 1$ transmitted data, ρ is average received power and $\mathbf{n}$ is the vector of independent and identically distributed complex $N(0, \sigma_n)$ noise.

The high propagation loss characteristics of mmWave channel causes limited scattering in the environment. Therefore, narrowband clustered channel model is more accurate for mmWave systems [7], [36]–[38]. Using the clustered channel model, channel matrix $\mathbf{H}$ can be expressed as summation of scattering components which consist of N_{cl} number of clusters and N_{ray} number of rays in each cluster. Considering that, the channel matrix $\mathbf{H}$ can be written as

$$\mathbf{H} = \sqrt{\frac{N_t N_r}{N_{cl} N_{ray}}} \sum_{i=1}^{N_{cl}} \sum_{k=1}^{N_{ray}} \alpha_{i,k} \mathbf{a}_r(\phi_{i,k}) \mathbf{a}_t^H(\theta_{i,k}), \quad (3)$$

where $\alpha_{i,k}$ is the complex gain of the k^{th} ray in the i^{th} cluster, $\mathbf{a}_t(\theta_{i,k})$ is the transmit antenna array response vector which is evaluated for $\theta_{i,k}$ departure angle of k^{th} ray in the i^{th} cluster, $\mathbf{a}_r(\phi_{i,k})$ is the receiver antenna array response vector which is evaluated for $\phi_{i,k}$ arrival angle of k^{th} ray in the i^{th} cluster. The N element array vector for TAs can be expressed as

$$\mathbf{a}(\theta_{i,k}) = \left[1 \quad \ldots \quad e^{-j\pi n \sin(\theta)} \quad \ldots \quad e^{-j\pi(N-1)\sin(\theta)}\right]^T. \quad (4)$$

Since the receiver implements a hybrid combiner $\mathbf{W}$ to the received signal, the processed received signal vector can be written as

$$\mathbf{y} = \sqrt{\rho}\mathbf{W}^H\mathbf{H}\mathbf{F}\mathbf{s} + \mathbf{W}^H\mathbf{n} \quad (5)$$

where $\mathbf{W}$ is the $N_r \times N_s$ receiver combining matrix. Considering $\mathbf{F}_{Lens}$ transmitter lens effect and hybrid precoding matrices, the precoding matrix $\mathbf{F}$ can be expanded as

$$\mathbf{F} = \mathbf{F}_{Lens}^{\mathbf{m}_t}\mathbf{F}_{RF}\mathbf{F}_{BB}, \quad (6)$$

where $\mathbf{m}_t$ represents $1 \times L_t$ vector of selected antenna indexes under each lens at the transmitter, $\mathbf{F}_{Lens}^{\mathbf{m}_t}$ is the $N_t \times L_t$ lens antenna effect, $\mathbf{F}_{RF}$ is the $L_t \times N_t^{RF}$ RF precoder using phase shifters at the transmitter, and $\mathbf{F}_{BB}$ is the $N_t^{RF} \times N_s$ digital precoder. Each column of $\mathbf{F}_{Lens}^{\mathbf{m}_t}$ matrix consist of zeros and $\mathbf{v}^m$. It can be expressed as

$$\mathbf{F}_{Lens}^{\mathbf{m}_t} = \begin{bmatrix} \mathbf{v}^{\mathbf{m}_t(1)} & \mathbf{0}_{M\times 1} & \ldots & \mathbf{0}_{M\times 1} \\ \mathbf{0}_{M\times 1} & \mathbf{v}^{\mathbf{m}_t(2)} & \mathbf{0}_{M\times 1} & \\ \vdots & & \ddots & \\ \mathbf{0}_{M\times 1} & \ldots & \mathbf{0}_{M\times 1} & \mathbf{v}^{\mathbf{m}_t(L_t)} \end{bmatrix}_{N_t \times L_t}. \quad (7)$$

The zeros in the matrix indicates that there is no contribution between subarrays to their individual beams that they generate. For a clear understanding of $\mathbf{F}_{Lens}^{\mathbf{m}_t}$ an example matrix with $M = 3$, $L = 2$, and $N = ML = 6$ can be given as

$$\mathbf{F}_{Lens}^{\mathbf{m}_t} = \begin{bmatrix} e^{j\pi M\sin(-\pi/4)} & 0 \\ 1 & 0 \\ e^{-j\pi M\sin(-\pi/4)} & 0 \\ 0 & 1 \\ 0 & 1 \\ 0 & 1 \end{bmatrix} \quad (8)$$

where $\mathbf{m}_t$ is selected as $[3, 2]$ which means that first LAS is excited by the 3rd antenna element radiating towards $\theta_3 = -\pi/4$ while second LAS is excited by the 2nd antenna element radiating towards $\theta_2 = 0$. Similarly, the combining matrix $\mathbf{W}$ can be written as

$$\mathbf{W} = \mathbf{W}_{Lens}^{\mathbf{m}_r}\mathbf{W}_{RF}\mathbf{W}_{BB}, \quad (9)$$

This work is licensed under a Creative Commons Attribution 4.0 License. For more information, see https://creativecommons.org/licenses/by/4.0/

This article has been accepted for publication in a future issue of this journal, but has not been fully edited. Content may change prior to final publication. Citation information: DOI 10.1109/ACCESS.2020.3041633, IEEE Access

where $\mathbf{m}_r$ represents vector of selected antenna indexes under each lens at the receiver, and $\mathbf{W}_{Lens}^{\mathbf{m}_r}$ is the $N_r \times L_r$ lens antenna effect, $\mathbf{W}_{RF}$ is the $L_r \times N_r^{RF}$ RF combiner using phase shifters at the receiver, and $\mathbf{W}_{BB}$ is the $N_r^{RF} \times N_s$ digital domain combining matrix.$\mathbf{W}_{Lens}^{\mathbf{m}_r}$ matrix can also be formed similarly to $\mathbf{F}_{Lens}^{\mathbf{m}_t}$ matrix by replacing transmitter domain variables with receiver domain variables.

Equation (5) represents all the antenna, RF processing, and digital processing of the system consisting of LAS architecture. Using this equation, the link throughput of the system can be calculated similarly to [14] as

$$R = \log_2 \left(\mathbf{I}_{N_s} + \frac{\rho}{N_s} \mathbf{R}_n^{-1} \mathbf{W}^H \mathbf{H} \mathbf{F} \mathbf{F}^* \mathbf{H}^* \mathbf{W} \right). \quad (10)$$

where $\mathbf{I}_{N_s}$ is $N_s \times N_s$ identity matrix, $\mathbf{R}_n = \sigma^2 \mathbf{W}^H \mathbf{W}$ is the noise covariance matrix after combining. However, finding an optimal precoding and combining matrices of $\{\mathbf{F}_{Lens}^{\mathbf{m}_t}, \mathbf{F}_{RF}, \mathbf{F}_{BB}, \mathbf{W}_{Lens}^{\mathbf{m}_r}, \mathbf{W}_{RF}, \mathbf{W}_{BB}\}$ is unlikely due to the non-convex constrains on discrete elements of $\{\mathbf{F}_{Lens}^{\mathbf{m}_t}, \mathbf{F}_{RF}, \mathbf{W}_{Lens}^{\mathbf{m}_r}, \mathbf{W}_{RF}\}$. Thus, to show the performance of proposed LAS concept, exhaustive search has been implemented during performance analysis to find efficient precoding and combining matrices. Details of exhaustive search procedure is given in Algorithm 1.

Algorithm 1: Exhaustive search procedure

Result: $\mathbf{F}_{Lens}, \mathbf{F}_{RF}, \mathbf{F}_{BB}, \mathbf{W}_{Lens}, \mathbf{W}_{RF}, \mathbf{W}_{BB}$
for *each* $\mathbf{m}_t$, $\mathbf{m}_r$ **do**
  for *each* $\mathbf{F}_{RF}$, $\mathbf{W}_{RF}$ **do**
    Calculate effective channel between Tx and Rx RF chains: $\tilde{\mathbf{H}} = \mathbf{W}^H \mathbf{H} \mathbf{F}$;
    Using singular value decomposition find optimum weights [14]: $\mathbf{F}_{BB} = \mathbf{F}_{opt}$
    $\mathbf{W}_{BB} = \left(\mathbf{F}_{opt}^H \tilde{\mathbf{H}}^H \tilde{\mathbf{H}} \mathbf{F}_{opt} + \sigma^2 N_s \mathbf{I}_{N_s} \right)^{-1} \mathbf{F}_{opt}^H \tilde{\mathbf{H}}^H$;
    Calculate R
  end for
end for
Pick $\mathbf{F}_{Lens}, \mathbf{F}_{RF}, \mathbf{W}_{Lens}, \mathbf{W}_{RF}$ that gives maximum R and their corresponding $\mathbf{F}_{BB}, \mathbf{W}_{BB}$;

III. PERFORMANCE ANALYSIS

In this section, we first provide a power consumption model for TA and LAS architecture. Subsequently, we investigate spectrum efficiency of these architectures with the system model presented in previous section. Finally, we evaluate the energy efficiency using the ratio of spectrum efficiency and power consumption.

A. POWER CONSUMPTION

Power consumption in traditional and alternative hybrid MIMO architectures has been investigated [17], [39] by considering the number of total hardware components (e.g. phase shifters, switches) and typical power consumption expected from these components. Reference [17] also presents a survey of hardware components developed for 60 GHz band applications. A wide range of power consumption values are typically observed and power consumption of particular hardware is selected based on certain justifications such as average value and expected trend in future years. We take a similar approach at the component level to evaluate and compare the power consumption of the LAS architecture and TA. First, these architectures are compared by assuming a single RF chain and ADC/DAC, i.e. architectures in Fig. 1 with $N^{RF} = 1$. We set the desired effective isotropic radiated power (EIRP) to 45 dBm based on existing/expected standards. We calculate the peak broadside gain of the traditional linear antenna array (G_{TA}) by assuming a 90% aperture efficiency (η_{TA}) as

$$G_{TA} = (4\pi/\lambda^2) A_p \eta_{TA}, \quad (11)$$

where A_p stands for the footprint area. A_p is linearly proportional to the element number N and element spacing d that is taken as $d = \lambda/2$ with λ representing the free space wavelength. The aperture efficiency of extended hemispherical or slab dielectric lenses used in [30], [35] can be as high as patch antenna arrays when compared with respect to the "footprint of lens base ($= A_p$)". Due to the lens/air mismatch and attractiveness of using low-cost (but with slightly higher loss) materials such as Acrynolitrile Butadiene Styrene (ABS) in 3D printing, aperture efficiency of LAS (η_{LAS}) is set to 80% and its gain is evaluated as

$$G_{LAS} = (4\pi/\lambda^2) A_p \eta_{LAS}. \quad (12)$$

To be similar with the antenna presented in [30], we set frequency to 38 GHz and take physical aperture area as $A_p = (N * 4) * 4$ mm^2, where 4 mm is a rounded value for the half of the free space wavelength $\lambda = 7.8947$ mm.

1) Transmitter Power Consumption

To achieve the desired EIRP (given in dBm), the total RF power that must be transmitted from the antenna elements can be expressed as

$$P_{T_x}^{TA} = 10^{0.1\text{EIRP}} / G_{TA} \quad (13)$$

$$P_{T_x}^{LAS} = 10^{0.1\text{EIRP}} / G_{LAS} \quad (14)$$

For the TA architecture consisting of single RF chain ($N^{RF} = 1$), the number of phase shifters is equal to the total number of antenna elements (i.e. $N_{PS} = N$). By representing the efficiency of the transmit amplifier with η_{PA}, DC power consumption of a phase shifter with P_{PS} and DC power consumption of an RF chain connected to ADC/DAC with P_C, the expression for the DC power consumption of TA becomes

$$P_{TA_t} = P_{T_x}^{TA} / \eta_{PA} + N P_{PS} + P_C. \quad (15)$$

This work is licensed under a Creative Commons Attribution 4.0 License. For more information, see https://creativecommons.org/licenses/by/4.0/

This article has been accepted for publication in a future issue of this journal, but has not been fully edited. Content may change prior to final publication. Citation information: DOI 10.1109/ACCESS.2020.3041633, IEEE Access

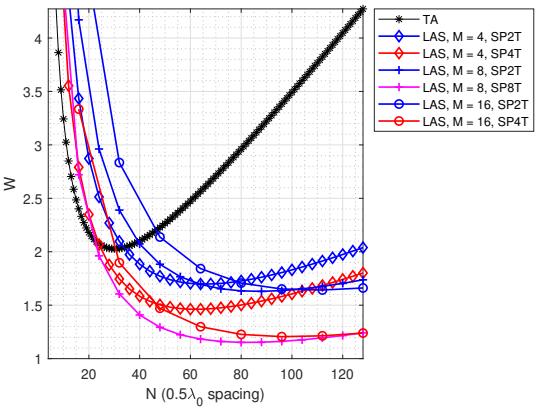


FIGURE 3. Power consumption of Lens Antenna Subarray (LAS) and Traditional (TA) hybrid MIMO architectures with single RF chain.

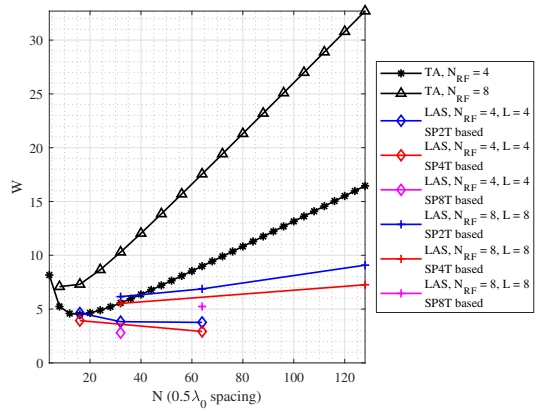


FIGURE 4. Power consumption of LAS and TA architectures with multiple RF chains ($N^{RF} \neq 1$).

In this equation, the insertion loss (IL) of N-way power dividers within the architecture is not modeled as in [17]. LAS architecture can potentially provide further advantage in this perspective since switches also perform power division. Phase shifters are in general implemented as active or passive devices. Passive phase shifters exhibit negligible power consumption, however, they are in need of amplifier to compensate for their high losses.

For the LAS architecture consisting of single RF chain ($N^{RF} = 1$), equation (15) must be modified to account for IL and DC power consumption of the switch network. The switch network performs single pole multiple throw functionality (SP(M)T). It can be implemented in various ways depending on choice of M in architecture. Here, we consider using SP2T, SP4T, and SP8T switches for $M = 4, 8$, and 16 where SP(K)T indicates single pole K throw. We assume the switch network's loss as $IL_{SW} = \ell * 1$ dB [40]–[42], where ℓ stands for the number of switches in series within the network . The IL introduced by the SP2T implementations will be higher due to the need for using multiple switches in series. For example, to support $M = 8$ antennas, an SP8T switch functionality is needed. This functionality can be implemented with a total of 7 SP2T switches. In this case, the RF signal arriving to a selected antenna element passes through 3 SP2T switches in series. Hence, $\ell = 3$ and the total loss of the SP8T switch network implemented with SP2T switches is $IL_{SW} = 3$ dB. Accounting for the switches, the DC power consumption of the LAS architecture becomes

$$P_{LAS_t} = \frac{P_{T_x}^{LAS}}{\eta_{PA}\eta_{SW}} + LP_{PS} + LN_{SW}P_{SW} + P_C. \quad (16)$$

where $\eta_{SW} = 10^{(-IL_{SW}/10)}$ stands for the efficiency of the switch network and P_{SW} represents the DC power consumption of the switch. The curves shown in Fig. 3 are generated with $\eta_{PA} = 0.2$, $P_{PS} = 30$ mW, and $P_C = 220mW$. As in [17], [22], P_C is taken significantly higher than P_{PS}. P_{PS} is based on commercially available phase shifters. P_{SW} is taken significantly lower as $P_{SP2T} = 10$ mW. For power consumption of larger throw switches, we use $P_{SP4T} = 20$ mW and $P_{SP8T} = 40$ mW. Fig. 3 demonstrates that for small arrays with $N < 30$, the efficiency of amplifiers dominate the power consumption. However, for larger arrays, power consumption in control components is the dominant contributor and larger lenses with more multiple throw switches offer better power savings. This can be explained from (13) and (14) where the output power of the PAs is calculated in order to provide the desired EIRP at 45 dBm. Since the array gains in the equations increase with the number of antenna elements, amplifiers consume less DC power in larger arrays. On the other hand, overall power consumption in (16) is formed by superposition of power consumption in amplifiers and control elements. With increasing number of antennas first the total power consumption drops due to power consumption of the amplifiers dominating equation (16). After reaching to enough antennas, the power consumption starts to increase with number of antennas because inclusion of more control components makes the power consumed by these components dominant term in (16). Different power consumption assumptions for the components produces similar trends demonstrating that large antenna arrays will benefit from the LAS architecture in terms of total power consumption.

Equations (15) and (16) can be generalized to multiple RF chains as

$$P_{TA_t}^{N^{RF}} = \frac{P_{T_x}^{TA}}{\eta_{PA}} + N^{RF}NP_{PS} + N^{RF}P_C, \quad (17)$$

$$P_{LAS_t}^{N^{RF}} = P_{T_x}^{LAS}/(\eta_{PA}\eta_{SW}) + N^{RF}LP_{PS} + N^{RF}LN_{SW}P_{SW} + N^{RF}P_C. \quad (18)$$

Fig. 4 depicts that the TA power consumption becomes heavily dominated by the phase shifters with increasing N^{RF}. For instance, for $N = 64$ the power consumption for $N^{RF} = 4$ and $N^{RF} = 8$ TA are 9 W and 18 W, respectively. Significant power savings can be achieved by the LAS architecture even in small array settings. For example, the power consumption ratio between TA and LAS architecture is $> 2:1$ for $N = 64$ and $N^{RF} = 8$ when LAS architecture is implemented with

This work is licensed under a Creative Commons Attribution 4.0 License. For more information, see https://creativecommons.org/licenses/by/4.0/

This article has been accepted for publication in a future issue of this journal, but has not been fully edited. Content may change prior to final publication. Citation information: DOI 10.1109/ACCESS.2020.3041633, IEEE Access

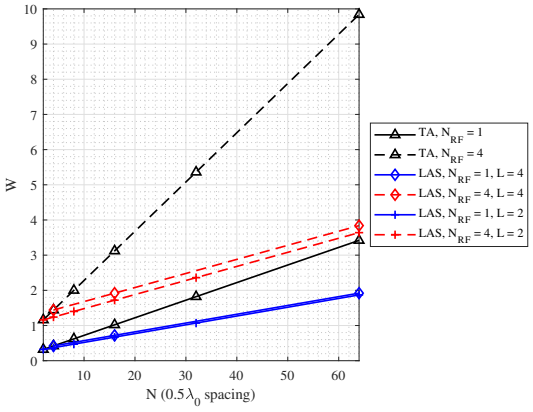


FIGURE 5. Power consumption of LAS and TA architectures when they are in receiving mode.

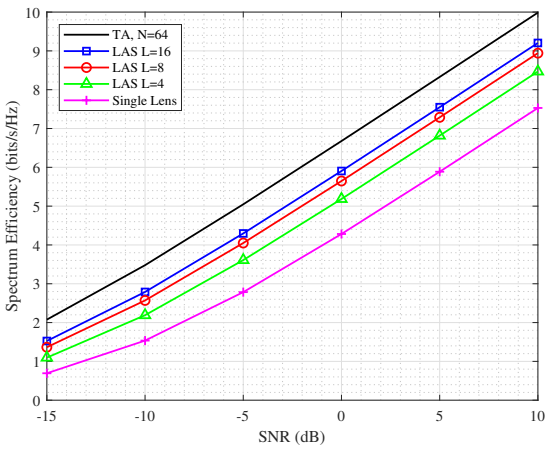


FIGURE 6. Spectrum efficiency of LAS and TA architectures with single RF chain when receiver is equipped with omni-directional antenna.

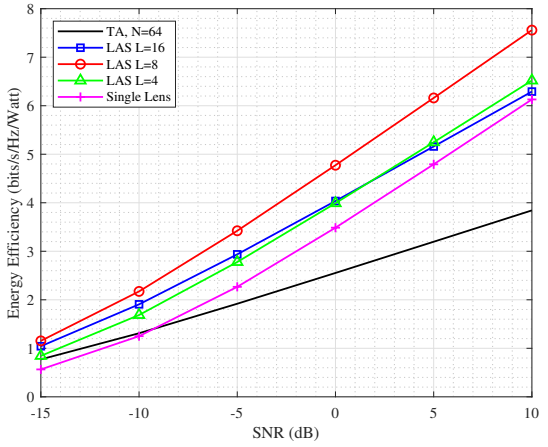


FIGURE 7. Energy efficiency of LAS and TA architectures with single RF chain when receiver is equipped with omni-directional antenna.

$M = 16$ elements per lens, $L = N/M = 4$ lenses and SP4T switches.

2) Receiver Power Consumption

Receiving architectures will employ low noise amplifiers (LNAs) at the antenna elements. Therefore, the power consumption model can be expressed by replacing transmitted RF power related quantities in equations (17) and (18) with LNA power consumption P_{LNA} as

$$P_{TA_r}^{N^{RF}} = NP_{LNA} + N^{RF}NP_{PS} + N^{RF}P_C, \quad (19)$$

$$P_{LAS_r}^{N^{RF}} = NP_{LNA} + N^{RF}LP_{PS} + N^{RF}LN_{SW}P_{SW} + N^{RF}P_C. \quad (20)$$

Fig. 5 shows $P_{TA_r}^{N^{RF}}$ and $P_{LAS_r}^{N^{RF}}$ as a function of N and N^{RF} with $P_{LNA} = 20$ mW [17]. It is observed that for multiple RF chains, the LAS architecture again presents significant reduction in power consumption.

B. SPECTRUM AND ENERGY EFFICIENCY

To evaluate the performance of the TA and LAS architecture, a scattering propagation channel is assumed. The propagation environment is modeled consisting of $N_{cl} = 6$ clusters with $N_{ray} = 8$ rays per cluster which are distributed on azimuth angles with Laplacian distribution as already utilized to model mmWave wireless communications in [36], [37]. For simplicity, all the clusters are assumed to have equal powers. The angular spread at both transmitter and receiver are distributed with the same variance. The channel is assumed to be known. The channel estimation can be performed with combination of similar approaches presented in [17], [43]–[46], but LAS may potentially benefit from a different channel estimation approach and this is beyond the scope of this manuscript. SNR is calculated as SNR $= \rho/\sigma_n^2$. Finally, all the reported results are averaged over 500 random channel realizations.

Fig. 6 and Fig. 7 show the spectrum and energy efficiency performances for $N^{RF} = 1$ scenario employing a transmitter consisting of $N_t = 64$ antenna elements while the receiver is equipped with an omni-directional antenna. When compared to SLA ($L = 1$), which can be referred as conventional beamspace MIMO, the LAS architecture provides increased spectrum efficiency. Specifically, the spectrum efficiency is improved by 15%, 24%, and 28% for $L = 4$, $L = 8$, and $L = 16$, respectively at SNR $= 5$dB. Due to its reduced precoding capability, the LAS architecture cannot reach to the spectrum efficiency performance of the TA which improves by 41% as compared to the SLA. However, these values still implies that spectrum efficiency of the LAS architecture is within 91% of TA for $L = 16$. Despite this minimal penalty in spectrum efficiency, the LAS architecture outperforms all other architectures in energy efficiency as seen in Fig. 7. Specifically, the energy efficiency of the LAS architecture is 161% of the TA for $L = 16$. It is important to note that the best energy efficient architecture in Fig. 7 is with $L = 8$ with 194% of the TA, showing the importance of making

This work is licensed under a Creative Commons Attribution 4.0 License. For more information, see https://creativecommons.org/licenses/by/4.0/

This article has been accepted for publication in a future issue of this journal, but has not been fully edited. Content may change prior to final publication. Citation information: DOI 10.1109/ACCESS.2020.3041633, IEEE Access

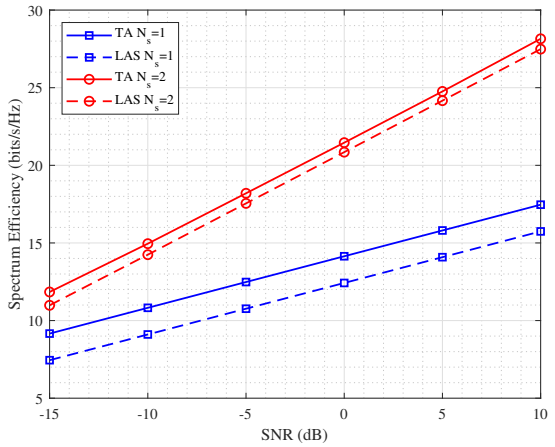


FIGURE 8. Spectrum efficiency of LAS and TA architectures with multiple RF chains and data streams. For LAS modeling, both transmitter and receiver are equipped with LAS.

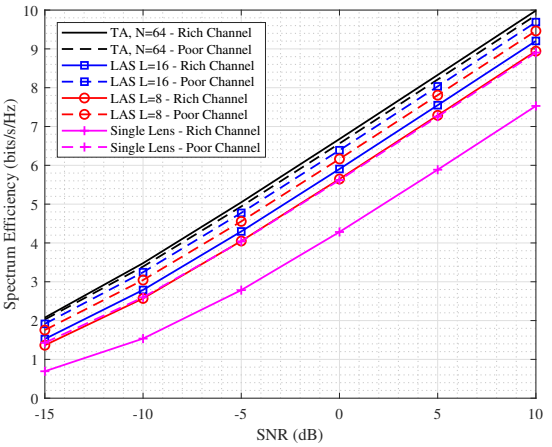


FIGURE 10. Spectrum efficiency of LAS and TA architectures for rich and poor channel scaterring scenarios when receiver is equipped with omni-directional antenna.

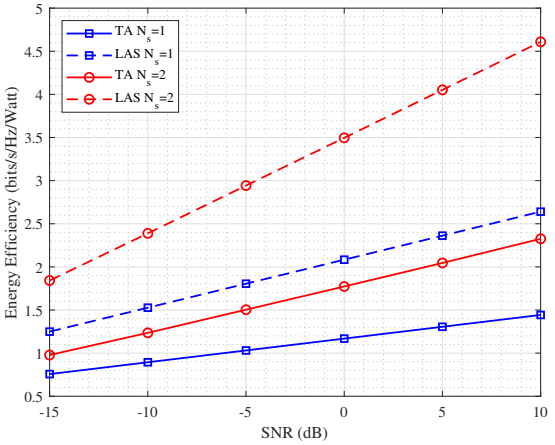


FIGURE 9. Energy efficiency of LAS and TA architectures with multiple RF chains and data streams. For LAS modeling, both transmitter and receiver are equipped with LAS.

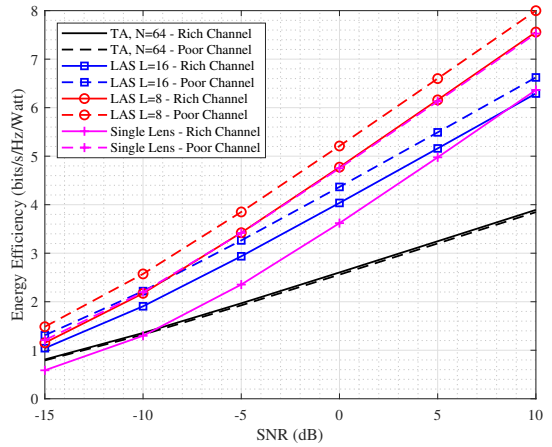


FIGURE 11. Energy efficiency of LAS and TA architectures for rich and poor channel scaterring scenarios when receiver is equipped with omni-directional antenna.

a careful trade-off between precoding gain and and power consumption in the LAS architecture design.

Fig. 8 and Fig. 9 show the spectrum and energy efficiency performances for multiple RF chain scenarios. Transmitter is assumed to employ $N_t = 64$ antenna elements, and $L_t = 16$ lenses with $N_t^{RF} = 8$ RF chains. Receiver is assumed to be equipped with $N_r = 16$ antenna elements, $L_r = 4$ lenses, and $N_r^{RF} = 4$ RF chains. The system is evaluated for 1 and 2 simultaneous streaming data cases to evaluate multiplexing effects as well. As seen in Fig. 8, the LAS architecture performs within 89% and 98% of the spectrum efficiency of the TA for 1 and 2 streaming data cases, respectively. Based on Fig. 9, energy efficiency of the LAS architecture is significantly better than the TA. Specifically, energy efficiency of the LAS architecture is 181% and 198% of that of the TA.

Fig. 10 and Fig. 11 show the performance under different scattering channel scenarios when $N^{RF} = 1$. A rich scattering channel is implemented with $N_{cl} = 12$ clusters and $N_{ray} = 16$ rays per cluster, while a poor scattering channel is implemented as $N_{cl} = 2$ clusters and $N_{ray} = 2$ rays per cluster. These selections can be interpreted as if the rich channel has 192 and the poor channel has 4 scatterers, respectively. As seen in Fig. 10 the LAS architecture performs better in a poor scattering environment as compared to a rich scattering environment. Its performance gets even closer to the TA in poor scattering channel conditions. This observation is also true for the SLA. However, both LAS architecture and TA outperforms the SLA in rich and poor scattering channels. Most importantly, it is observed that SLA suffers the most in a rich scattering environment, while the LAS architecture still can perform close to a TA within 90% of spectrum efficiency for $L = 16$. Fig. 10 also shows that the LAS architecture slightly performs worse in a rich scattering channel as compared to poor scattering channel. This is related to the limited

This work is licensed under a Creative Commons Attribution 4.0 License. For more information, see https://creativecommons.org/licenses/by/4.0/

This article has been accepted for publication in a future issue of this journal, but has not been fully edited. Content may change prior to final publication. Citation information: DOI 10.1109/ACCESS.2020.3041633, IEEE Access

TABLE 1. Performance comparison of LAS architecture with TA when SNR $= 5$ dB, see Section III.A for power consumption model and assumptions, $L_t = 8$ for $N_t^{RF} = 1$ and $L_t = 16$ for $N_t^{RF} = 8$.

(bits/s/Hz)	$N_t = 64$	**TA**	**SLA**	**LAS (This Work)**
Data Rate	$N_s = 1$ $N_t^{RF} = 1$	8.33	5.89 71% of TA	7.29 88% of TA
	$N_s = 2$ $N_t^{RF} = 8$	24.76	-	24.16 98% of TA
Energy Efficiency (per Watt)	$N_s = 1$ $N_t^{RF} = 1$	3.2	4.8 150% of TA	6.2 194% of TA
	$N_s = 2$ $N_t^{RF} = 8$	2.05	-	4.05 198% of TA
Poor Channel	$N_s = 1$ $N_t^{RF} = 1$	8.21	7.25 88% of TA	7.8 95% of TA
Rich Channel	$N_s = 1$ $N_t^{RF} = 1$	8.33	5.89 71% of TA	7.29 88% of TA

precoding capability of the architecture as compared to TA. When the signal arrives from too many multipath directions, the LAS architecture will not be able to adapt the antenna gain pattern as flexibly as TA can do. The pattern created by an antenna group (i.e. M elements) behind a lens cannot be optimized by changing antenna coefficients. Only the pattern direction can be changed by selecting the antenna element exciting the lens. Due to this reason, the SLA suffers most as it does not exhibit any precoding capability since all antenna elements are behind the lens with no capability of pattern optimization by changing antenna coefficients.

Fig. 11 shows that the energy efficiency of the LAS architecture again outperforms the TA approach by about 100% in rich or poor scattering channel conditions. This is again due to the close spectrum efficiency between the two architectures, but significantly reduced power consumption in the LAS architecture. Finally, Table 1 presents the summary of the observations that has been made during the performance evaluation of the LAS architecture throughout this manuscript.

Although channel estimation is beyond the scope of this manuscript, it is possible to perform a convenient investigation of spectrum and energy efficiency performance of the LAS architecture under imperfect channel knowledge by making use of mean square error (MSE) performance of channel estimation from prior references. Reference [43] investigates a scattering propagation environment with $N_{cl} = 2$ clusters with $N_{ray} = 1$ ray per cluster. Fig. 12 and Fig. 13 show the performance of the LAS architecture with the MSE performance of the presented channel estimation algorithm in [43] for $N^{RF} = 1$ scenario employing a transmitter consisting of $N_t = 64$ antenna elements while the receiver is equipped with an omni-directional antenna. As it can be seen from the figures, LAS and SLA architectures suffer similarly in spectrum and energy efficiency performance under imperfect channel knowledge. In energy efficiency, the LAS architecture operating with imperfect channel knowledge

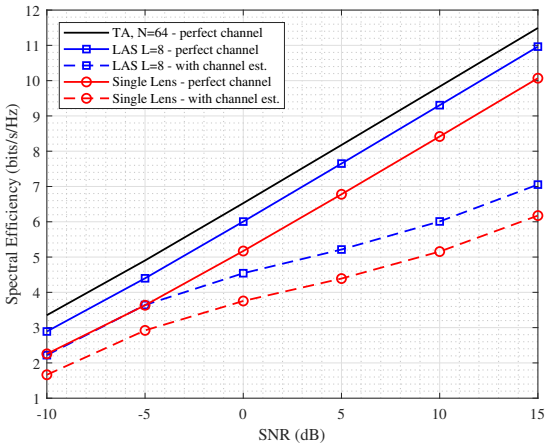


FIGURE 12. Spectrum efficiency comparison of LAS and TA architectures under imperfect channel knowledge

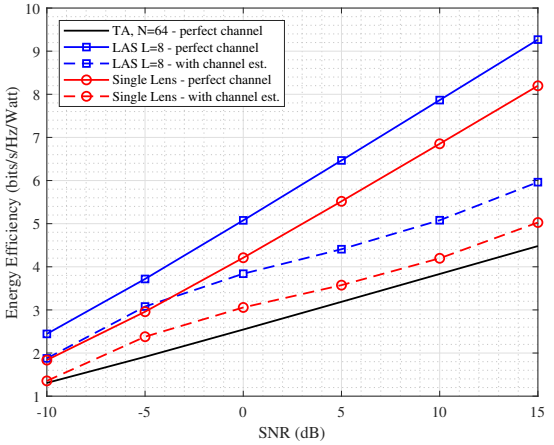


FIGURE 13. Energy efficiency comparison of LAS and TA architectures under imperfect channel knowledge

can even outperform a TA operating with perfect channel knowledge.

IV. CONCLUDING REMARKS

Spectrum and energy efficiencies of mmWave wireless communication systems consisting of a new LAS based hybrid MIMO architecture were investigated. The LAS architecture was shown to provide improved energy efficiency while providing similar spectrum efficiency to TA. For example in a system with $N_s = 2$ data stream transmissions, employing LAS architecture at the transmitter ($N_t = 64$ antennas, $L_t = 16$ lenses, $N_t^{RF} = 8$ RF chains) and at the receiver ($N_r = 16$ antennas, $L_r = 4$ lenses, $N_r^{RF} = 4$ RF chains) provides 98% of the data rate that can be achieved by the TA. On the other hand, in this scenario, the LAS architecture operates with 194% energy efficiency of the TA. As compared to SLA, the LAS architecture provides significant advantages in data rate and energy efficiency particularly in scatttering channel conditions that will be observed in mmWave bands.

This work is licensed under a Creative Commons Attribution 4.0 License. For more information, see https://creativecommons.org/licenses/by/4.0/

This article has been accepted for publication in a future issue of this journal, but has not been fully edited. Content may change prior to final publication. Citation information: DOI 10.1109/ACCESS.2020.3041633, IEEE Access

The presented system model used exhaustive search for precoding/combiner matrices and channel estimation was not performed. Future work will consider LAS architecture specific channel estimation and precoder/combiner estimation algorithms to investigate the performance towards practical system implementations. Multi-user scenarios will also be investigated along with antenna hardware implementations.

REFERENCES

[1] J. G. Andrews, S. Buzzi, W. Choi, S. V. Hanly, A. Lozano, A. C. K. Soong, and J. C. Zhang, "What will 5G be?" *IEEE Journal on Selected Areas in Communications*, vol. 32, no. 6, pp. 1065–1082, June 2014.

[2] T. S. Rappaport, S. Shu, R. Mayzus, Z. Hang, Y. Azar, K. Wang, G. N. Wong, J. K. Schulz, M. Samimi, and F. Gutierrez, "Millimeter wave mobile communications for 5G cellular: It will work!" *IEEE Access*, vol. 1, pp. 335–349, 2013.

[3] Federal Communications Commission, "FCC takes steps to facilitate mobile broadband and next generation wireless technologies in spectrum above 24 GHz," Tech. Rep., Jul. 2016. [Online]. Available: https://apps.fcc.gov/edocs_public/attachmatch/DOC-340301A1.pdf

[4] A. I. Sulyman, A. T. Nassar, M. K. Samimi, G. R. MacCartney, T. S. Rappaport, and A. Alsanie, "Radio propagation path loss models for 5G cellular networks in the 28 GHz and 38 GHz millimeter-wave bands," *IEEE Communications Magazine*, vol. 52, no. 9, pp. 78–86, 2014.

[5] M. Elkashlan, T. Q. Duong, and H.-H. Chen, "Millimeter-wave communications for 5G: fundamentals: Part I [guest editorial]," *IEEE Communications Magazine*, vol. 52, no. 9, pp. 52–54, 2014.

[6] W. Roh, J.-Y. Seol, J. Park, B. Lee, J. Lee, Y. Kim, J. Cho, K. Cheun, and F. Aryanfar, "Millimeter-wave beamforming as an enabling technology for 5g cellular communications: theoretical feasibility and prototype results," *IEEE Communications Magazine*, vol. 52, no. 2, pp. 106–113, feb 2014.

[7] S. Sun, T. Rappaport, R. Heath, A. Nix, and S. Rangan, "Mimo for millimeter-wave wireless communications: beamforming, spatial multiplexing, or both?" *IEEE Communications Magazine*, vol. 52, no. 12, pp. 110–121, dec 2014.

[8] T. S. Rappaport, F. Gutierrez, E. Ben-Dor, J. N. Murdock, Y. Qiao, and J. I. Tamir, "Broadband millimeter-wave propagation measurements and models using adaptive-beam antennas for outdoor urban cellular communications," *IEEE Transactions on Antennas and Propagation*, vol. 61, no. 4, pp. 1850–1859, April 2013.

[9] Y. Niu, Y. Li, D. Jin, L. Su, and A. V. Vasilakos, "A survey of millimeter wave communications (mmWave) for 5G: Opportunities and challenges," *Wireless Networks*, vol. 21, no. 8, pp. 2657–2676, 2015.

[10] A. Alkhateeb, J. Mo, N. Gonzalez-Prelcic, and R. W. Heath, "MIMO precoding and combining solutions for millimeter-wave systems," *IEEE Communications Magazine*, vol. 52, no. 12, pp. 122–131, dec 2014.

[11] F. Gholam, J. Via, and I. Santamaria, "Beamforming design for simplified analog antenna combining architectures," *IEEE Transactions on Vehicular Technology*, vol. 60, no. 5, pp. 2373–2378, 2011.

[12] S. Kutty and D. Sen, "Beamforming for millimeter wave communications: An inclusive survey," *IEEE Communications Surveys Tutorials*, vol. 18, no. 2, pp. 949–973, Secondquarter 2016.

[13] X. Zhang, A. Molisch, and S.-Y. Kung, "Variable-phase-shift-based RF-baseband codesign for MIMO antenna selection," *IEEE Transactions on Signal Processing*, vol. 53, no. 11, pp. 4091–4103, nov 2005.

[14] O. E. Ayach, S. Rajagopal, S. Abu-Surra, Z. Pi, and R. W. Heath, "Spatially sparse precoding in millimeter wave MIMO systems," *IEEE Transactions on Wireless Communications*, vol. 13, no. 3, pp. 1499–1513, mar 2014.

[15] J. G. Andrews, T. Bai, M. N. Kulkarni, A. Alkhateeb, A. K. Gupta, and R. W. Heath, "Modeling and analyzing millimeter wave cellular systems," *IEEE Transactions on Communications*, vol. 65, no. 1, pp. 403–430, Jan 2017.

[16] C. Rusu, R. Mendez-Rial, N. Gonzalez-Prelcic, and R. W. Heath, "Low complexity hybrid precoding strategies for millimeter wave communication systems," *IEEE Transactions on Wireless Communications*, vol. 15, no. 12, pp. 8380–8393, dec 2016.

[17] R. Mendez-Rial, C. Rusu, N. Gonzalez-Prelcic, A. Alkhateeb, and R. W. Heath, "Hybrid MIMO architectures for millimeter wave communications: Phase shifters or switches?" *IEEE Access*, vol. 4, pp. 247–267, 2016.

[18] A. Mezghani and J. A. Nossek, "On ultra-wideband MIMO systems with 1-bit quantized outputs: Performance analysis and input optimization," in *2007 IEEE International Symposium on Information Theory*, 2007, pp. 1286–1289.

[19] J. Mo, A. Alkhateeb, S. Abu-Surra, and R. W. Heath, "Hybrid architectures with few-bit ADC receivers: Achievable rates and energy-rate tradeoffs," *IEEE Transactions on Wireless Communications*, vol. 16, no. 4, pp. 2274–2287, 2017.

[20] A. Abbaspour-Tamijani and K. Sarabandi, "An affordable millimeter-wave beam-steerable antenna using interleaved planar subarrays," *IEEE Transactions on Antennas and Propagation*, vol. 51, no. 9, pp. 2193–2202, sep 2003.

[21] S. Park, A. Alkhateeb, and R. W. Heath, "Dynamic subarrays for hybrid precoding in wideband mmwave MIMO systems," *IEEE Transactions on Wireless Communications*, vol. 16, no. 5, pp. 2907–2920, 2017.

[22] S. He, C. Qi, Y. Wu, and Y. Huang, "Energy-efficient transceiver design for hybrid sub-array architecture MIMO systems," *IEEE Access*, vol. 4, pp. 9895–9905, 2016.

[23] Y. Sun, Z. Gao, H. Wang, B. Shim, G. Gui, G. Mao, and F. Adachi, "Principal component analysis-based broadband hybrid precoding for millimeter-wave massive MIMO systems," *IEEE Transactions on Wireless Communications*, vol. 19, no. 10, pp. 6331–6346, 2020.

[24] J. Brady, N. Behdad, and A. M. Sayeed, "Beamspace MIMO for millimeter-wave communications: System architecture, modeling, analysis, and measurements," *IEEE Transactions on Antennas and Propagation*, vol. 61, no. 7, pp. 3814–3827, jul 2013.

[25] Y. Zeng and R. Zhang, "Millimeter wave MIMO with lens antenna array: A new path division multiplexing paradigm," *IEEE Transactions on Communications*, vol. 64, no. 4, pp. 1557–1571, apr 2016.

[26] Y. J. Cho, G.-Y. Suk, B. Kim, D. K. Kim, and C.-B. Chae, "RF lens-embedded antenna array for mmWave MIMO: Design and performance," *IEEE Communications Magazine*, vol. 56, no. 7, pp. 42–48, jul 2018.

[27] W. Huang, Y. Huang, Y. Zeng, and L. Yang, "Wideband millimeter wave communication with lens antenna array: Joint beamforming and antenna selection with group sparse optimization," *IEEE Transactions on Wireless Communications*, vol. 17, no. 10, pp. 6575–6589, oct 2018.

[28] C. Feng, W. Shen, and J. An, "Beam selection for wideband millimeter wave MIMO relying on lens antenna arrays," *IEEE Communications Letters*, vol. 23, no. 10, pp. 1875–1878, oct 2019.

[29] Y. Zeng, L. Yang, and R. Zhang, "Multi-user millimeter wave MIMO with full-dimensional lens antenna array," *IEEE Transactions on Wireless Communications*, vol. 17, no. 4, pp. 2800–2814, apr 2018.

[30] G. Mumcu, M. Kacar, and J. Mendoza, "Mm-wave beam steering antenna with reduced hardware complexity using lens antenna subarrays," *IEEE Antennas and Wireless Propagation Letters*, vol. 17, no. 9, pp. 1603–1607, sep 2018.

[31] M. Karabacak, G. Mumcu, and H. Arslan, "Hybrid MIMO architecture using lens arrays," U.S. Patent 10 714 836, July 14, 2020.

[32] M. Khalily, R. Tafazolli, T. A. Rahman, and M. R. Kamarudin, "Design of phased arrays of series-fed patch antennas with reduced number of the controllers for 28-GHz mm-Wave applications," *IEEE Antennas and Wireless Propagation Letters*, vol. 15, pp. 1305–1308, 2016.

[33] B. Avser, J. Pierro, and G. M. Rebeiz, "Random feeding networks for reducing the number of phase shifters in limited-scan arrays," *IEEE Transactions on Antennas and Propagation*, vol. 64, no. 11, pp. 4648–4658, 2016.

[34] F. Akbar and A. Mortazawi, "Scalable phased array architectures with a reduced number of tunable phase shifters," *IEEE Transactions on Microwave Theory and Techniques*, vol. 65, no. 9, pp. 3428–3434, 2017.

[35] K. Shila and G. Mumcu, "Mm-wave beam steering antenna based on extended hemispherical lens antenna subarrays," in *2020 IEEE International Symposium on Antennas and Propagation and USNC-URSI Radio Science Meeting*, Jul. 2020, pp. 1–2.

[36] A. Forenza, D. J. Love, and R. W. Heath, "Simplified spatial correlation models for clustered MIMO channels with different array configurations," *IEEE Transactions on Vehicular Technology*, vol. 56, no. 4, pp. 1924–1934, 2007.

[37] Hao Xu, V. Kukshya, and T. S. Rappaport, "Spatial and temporal characteristics of 60-GHz indoor channels," *IEEE Journal on Selected Areas in Communications*, vol. 20, no. 3, pp. 620–630, 2002.

[38] P. F. M. Smulders and L. M. Correia, "Characterisation of propagation in 60 GHz radio channels," *Electronics Communication Engineering Journal*, vol. 9, no. 2, pp. 73–80, 1997.

[39] A. Yazdan, J. Park, S. Park, T. A. Khan, and R. W. Heath, "Energy-efficient massive MIMO: Wireless-powered communication, multiuser MIMO with

This work is licensed under a Creative Commons Attribution 4.0 License. For more information, see https://creativecommons.org/licenses/by/4.0/

This article has been accepted for publication in a future issue of this journal, but has not been fully edited. Content may change prior to final publication. Citation information: DOI 10.1109/ACCESS.2020.3041633, IEEE Access

hybrid precoding, and cloud radio access network with variable-resolution ADCs," *IEEE Microwave Magazine*, vol. 18, no. 5, pp. 18–30, 2017.

[40] M. Lokhandwala, L. Gao, and G. M. Rebeiz, "A high-power 24–40-GHz transmit–receive front end for phased arrays in 45-nm CMOS SOI," *IEEE Transactions on Microwave Theory and Techniques*, vol. 68, no. 11, pp. 4775–4786, 2020.

[41] C. Li, O. Elaassar, N. Satish, A. Kumar, N. Cahoon, and G. Rebeiz, "5G mm-Wave SPDT switch IMDn investigation," in *IEEE MTT-S International Microwave Conference on Hardware and Systems for 5G and Beyond (IMC-5G)*, 2019, pp. 1–3.

[42] Qorvo, "High power Ka-band SPDT switch - TGS4302," May 2008. [Online]. Available: https://www.qorvo.com/products/p/TGS4302

[43] L. Yang, Y. Zeng, and R. Zhang, "Channel estimation for millimeter-wave MIMO communications with lens antenna arrays," *IEEE Transactions on Vehicular Technology*, vol. 67, no. 4, pp. 3239–3251, 2018.

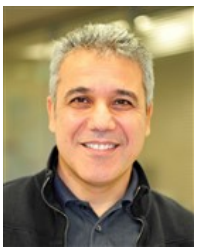
[44] L. Dai, X. Gao, S. Han, I. Chih-Lin, and X. Wang, "Beamspace channel estimation for millimeter-wave massive MIMO systems with lens antenna array," in *IEEE/CIC International Conference on Communications in China (ICCC)*, 2016, pp. 1–6.

[45] W. Ma and C. Qi, "Channel estimation for 3-D lens millimeter wave massive MIMO system," *IEEE Communications Letters*, vol. 21, no. 9, pp. 2045–2048, 2017.

[46] Z. Wan, Z. Gao, B. Shim, K. Yang, G. Mao, and M. Alouini, "Compressive sensing based channel estimation for millimeter-wave full-dimensional MIMO with lens-array," *IEEE Transactions on Vehicular Technology*, vol. 69, no. 2, pp. 2337–2342, 2020.



MURAT KARABACAK (GS'11-M'20) received his B.S. and M.Sc. degrees in Electrical and Electronics Engineering from Istanbul University, Istanbul, Turkey in 2008 and 2010, respectively. He is currently pursuing his Ph.D. degree in Electrical Engineering at the University of South Florida. In 2013, he was with the research group of NTT Docomo Inc., CA, USA, as an intern where he was involved in the research of mobility, load balancing, analog beamforming in small cells. His research interests are physical and medium access control layer algorithms on beamforming, mobility management, initial access, and self-organization in cellular networks for optimization of efficient control in wireless networks.



HÜSEYIN ARSLAN (IEEE Fellow, IEEE Distinguished Lecturer) received his BS degree from the Middle East Technical University (METU), Ankara, Turkey in 1992; his MS and Ph.D. degrees were received respectively in 1994 and 1998 from Southern Methodist University (SMU), Dallas, TX. From January 1998 to August 2002, he was with the research group of Ericsson, where he was involved with several projects related to 2G and 3G wireless communication systems. Since August 2002, he has been with the Electrical Engineering Department, at the University of South Florida, where he is a Professor. In December 2013, he joined Istanbul Medipol University to found the Engineering College, where he has worked as the Dean of the School of Engineering and Natural Sciences. In addition, he has worked as a part-time consultant for various companies and institutions including Anritsu Company and The Scientific and Technological Research Council of Turkey.

Dr. Arslan conducts research in wireless systems, with emphasis on the physical and medium access layers of communications. His current research interests are on 5G and beyond radio access technologies, physical layer security, interference management (avoidance, awareness, and cancellation), cognitive radio, multi-carrier wireless technologies (beyond OFDM), dynamic spectrum access, co-existence issues, non-terrestial communications (High Altitude Platforms), joint radar (sensing) and communication designs. Dr. Arslan has been collaborating extensively with key national and international industrial partners and his research has generated significant interest in companies such as InterDigital, Anritsu, NTT DoCoMo, Raytheon, Honeywell, Keysight technologies. Collaborations and feedback from industry partners has significantly influenced his research. In addition to his research activities, Dr. Arslan has also contributed to wireless communication education. He has integrated the outcomes of his research into education which lead him to develop a number of courses at the University of South Florida. He has developed a unique "Wireless Systems Laboratory" course (funded by the National Science Foundation and Keysight technologies) where he was able to teach not only the theory but also the practical aspects of wireless communication system with the most contemporary test and measurement equipment.

Dr. Arslan has served as general chair, technical program committee chair, session and symposium organizer, workshop chair, and technical program committee member in several IEEE conferences. He is currently a member of the editorial board for the IEEE Surveys and Tutorials and the Sensors Journal. He has also served as a member of the editorial board for the IEEE Transactions on Communications, the IEEE Transactions on Cognitive Communications and Networking (TCCN), and several other scholarly journals by Elsevier, Hindawi, and Wiley Publishing.

This work is licensed under a Creative Commons Attribution 4.0 License. For more information, see https://creativecommons.org/licenses/by/4.0/

This article has been accepted for publication in a future issue of this journal, but has not been fully edited. Content may change prior to final publication. Citation information: DOI 10.1109/ACCESS.2020.3041633, IEEE Access



GOKHAN MUMCU (S'03–M'09–SM'15) was born in Bursa, Turkey, on March 30, 1982. He received the B.S. degree in electrical engineering from Bilkent University, Ankara, Turkey, in 2003, and the M.S. and Ph.D. degrees in electrical and computer engineering from The Ohio State University, Columbus, in 2005 and 2008, respectively.

He is currently an Associate Professor at the Electrical Engineering Department of University of South Florida, Tampa, FL. From 2009 to 2015, he was an Assistant Professor at the Electrical Engineering Department of University of South Florida. His research interests are additive manufacturing of antennas and phased antenna arrays, reconfigurable antennas and RF devices, microfluidics-based techniques for RF device and antenna reconfiguration, small antennas, and engineered materials.

Dr. Mumcu is the recipient of the 2014 CAREER award from the U.S. National Science Foundation. He is also recipient of 2014 faculty outstanding research award from the University of South Florida. He ranked first on the national university entrance exam taken annually by over 1.5 million Turkish students in 1999. He received the 1999 international education fellowship of the Turkish Ministry of Education. He was the recipient of a best paper award at 2008 URSI National Radio Science Meeting, and the 2008 outstanding dissertation award at The Ohio State University, ElectroScience Laboratory. He served as the technical program committee chairs of the 2013 IEEE International Symposium on Antennas and Propagation and USNC/URSI National Radio Science Meeting and 2016 International Workshop on Antenna Technology (iWAT).

This work is licensed under a Creative Commons Attribution 4.0 License. For more information, see https://creativecommons.org/licenses/by/4.0/